Macromolecules
Cite This: Macromolecules 2019, 52, 4464−4474
Article
pubs.acs.org/Macromolecules

Carboxylate-Substituted Polythiophenes for Efficient Fullerene-Free Polymer Solar Cells: The Effect of Chlorination on Their Properties

Qi Wang,[†] Miaomiao Li,*[,†,‡,§] Xiaowei Zhang,[†] Yunpeng Qin,[∥] Junke Wang,[§] Jidong Zhang,[⊥] Jianhui Hou,[∥] René A. J. Janssen,[§] and Yanhou Geng*[,†,‡]

[†]School of Materials Science and Engineering, Tianjin University, Tianjin 300072, P. R. China

[‡]Tianjin Key Laboratory of Molecular Optoelectronic Science, Tianjin University, and Collaborative Innovation Center of Chemical Science and Engineering (Tianjin), Tianjin 300072, P. R. China

[§]Molecular Materials and Nanosystems and Institute for Complex Molecular Systems, Eindhoven University of Technology, PO Box 513, 5600 MB Eindhoven, The Netherlands

[∥]Beijing National Laboratory for Molecular Science and State Key Laboratory of Polymer Physics and Chemistry, Institute of Chemistry, Chinese Academy of Sciences, Beijing 100190, P. R. China

[⊥]State Key Laboratory of Polymer Physics and Chemistry, Changchun Institute of Applied Chemistry, Chinese Academy of Sciences, Changchun 130022, P. R. China

Supporting Information

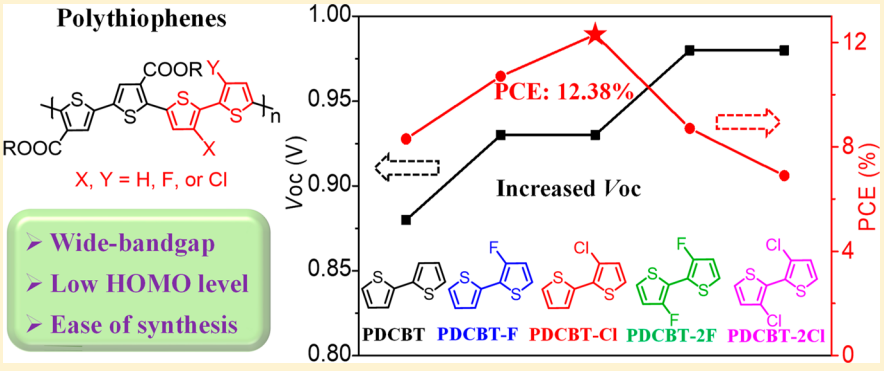

ABSTRACT: Two new wide-bandgap polythiophenes, i.e., poly[5,5′-bis(2-hexyldecyl)-(2,2′-bithiophene)-4,4′-dicarboxylate-*alt*-5,5′-3-chloro-2,2′-bithiophene] (PDCBT-Cl) and poly[5,5′-bis(2-hexyldecyl)-(2,2′-bithiophene)-4,4′-dicarboxylate-*alt*-5,5′-3,3′-dichloro-2,2′-bithiophene] (PDCBT-2Cl) comprising 3-chloro-2,2′-bithiophene and 3,3′-dichloro-2,2′-bithiophene moieties, respectively, were synthesized for fullerene-free polymer solar cells (PSCs). For comparison, three other polymers based on [2,2′-bithiophene]-4,4′-dicarboxylate (DCBT), i.e., PDCBT, PDCBT-F, and PDCBT-2F with 2,2′-bithiophene, 3-fluoro-2,2′-bithiophene, and 3,3′-difluoro-2,2′-bithiophene as comonomers, respectively, were also prepared. PSC devices were fabricated with these polymers as donor materials and ITIC-Th1 as acceptor. The incorporation of chlorine (Cl) or fluorine (F) atoms into polymers both efficiently downshifted the highest occupied molecular orbital (HOMO) energy levels, leading to higher open-circuit voltage (V_{oc}) in the PSCs. Owing to the proper phase-separated morphology with favorable molecular packing and miscibility, the device based on PDCBT-Cl:ITIC-Th1 exhibited efficient exciton dissociation and charge collection as well as weak charge recombination and thereby displayed the best power conversion efficiency (PCE) up to 12.38%. The devices based on other polymers showed inferior PCEs (8.14% for PDCBT, 10.85% for PDCBT-F, 8.48% for PDCBT-2F, and 6.94% for PDCBT-2Cl). The monomers that are used to make PDCBT-Cl can be synthesized in relatively large scale from commercial available chemicals. All these indicate that PDCBT-Cl is a promising donor material for the large area fabrication of high-performance fullerene-free PSCs.

INTRODUCTION

Polymer solar cells (PSCs) based on a blend of a semiconducting conjugated polymer donor and an electron acceptor have attracted enormous attention due to their advantages of low cost, flexibility, light weight, and solution based fabrication.[1−3] In the past few years, the power conversion efficiencies (PCEs) of PSCs have increased sharply because of the rapid development of non-fullerene acceptors (NFAs).[4−11] Unlike fullerene derivatives and perylene diimide based electron acceptors, the acceptor−donor−acceptor (A−

Received: April 17, 2019
Revised: May 27, 2019
Published: June 11, 2019

DOI: 10.1021/acs.macromol.9b00793
Macromolecules 2019, 52, 4464−4474

Chart 1. Chemical Structures of PDCBT, PDCBT-F, PDCBT-2F, PDCBT-Cl, PDCBT-2Cl, and ITIC-Th1

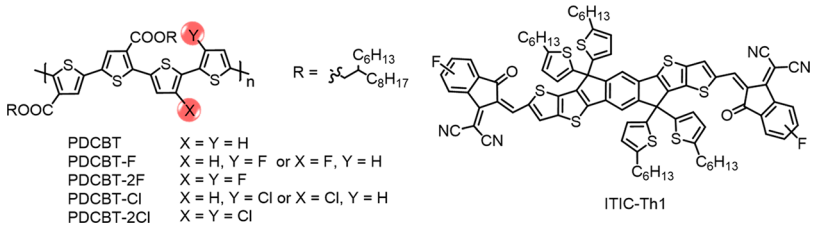

Scheme 1. Synthetic Routes to the Monomer DCBT-2Br and the Polymers[a]

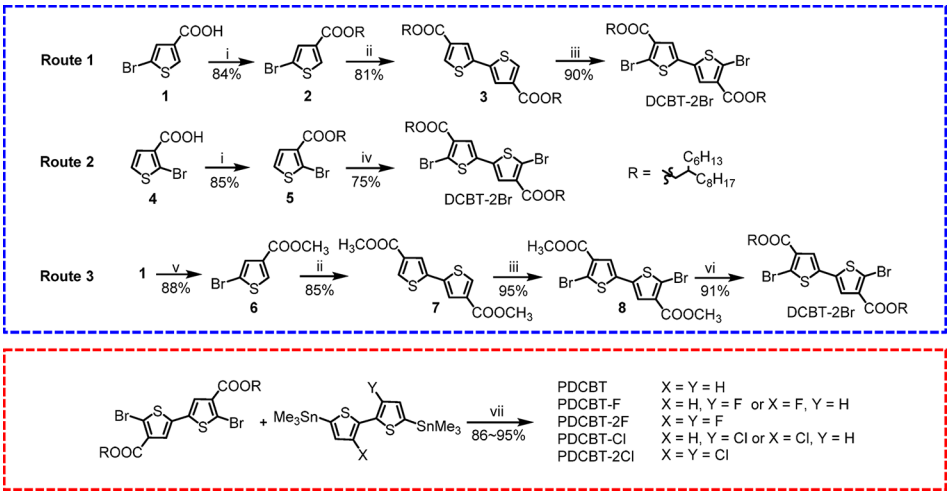

[a]Reagents and conditions: (i) 2-hexyl-1-decanol, DCC, DMAP, CH_2Cl_2, RT; (ii) bis(pinacolato)diboron, $Pd_2(dba)_3$, $HPCy_3BF_4$, CsF, dioxane, 80 °C; (iii) NBS, $CHCl_3/CF_3COOH$, RT; (iv) $Pd(PhCN)_2Cl_2$, $AgNO_3$, KF, DMSO, 60 °C; (v) TsOH, methanol, reflux; (vi) 2-hexyl-1-decanol, $Ti(acac)_2$, toluene, reflux; (vii) $Pd(PPh_3)_4$, chlorobenzene, 135 °C. DCC: *N*,*N*′-dicyclohexylcarbodiimide; DMAP: 4-(dimethylamino)pyridine.

D−A)-type fused-ring electron acceptors possess strong and broad absorption in the visible region, and the absorption spectra can be easily extended into the near-infrared (NIR) region via molecular design.[12−21] To pursue maximized photon harvesting, wide-bandgap (WBG, optical bandgap (E_g^{opt}) > 1.8 eV) donor polymers having complementary absorption with the medium-bandgap (1.6 < E_g^{opt} < 1.8 eV) and low-bandgap (E_g^{opt} < 1.6 eV) acceptors are highly desired. Recently, the PCEs of single-junction PSCs have reached 14%−16%, attributed to the rational design of the WBG polymer donors and A−D−A-type fused-ring NFAs.[19,22−28] Along with the improvement of PSC performance, easy accessibility of the photoactive materials is of importance to meet the future commercial applications of PSCs.[29,30]

Polythiophenes (PTs) are one of the most important types of WBG donor materials. As a representative of PTs, regioregular poly(3-hexylthiophene) (P3HT) is featured by low cost and ease of synthesis and plays an important role in the development of PSCs.[31−35] However, because of the strongly electron-rich characteristics of the thiophene unit, P3HT has a high-lying highest occupied molecular orbital (HOMO) energy level of ∼−4.9 eV, and hence it is difficult to obtain a high open-circuit voltage (V_{oc}) because the V_{oc} of PSCs is directly related to the difference between the lowest unoccupied molecular orbital (LUMO) energy level of the acceptor and HOMO energy level of the donor. To address this issue, electron-withdrawing groups, such as fluorine (F), carboxylate, and cyano, have been introduced to PT conjugated backbones to lower the HOMO energy level.[36−42] For example, Hou et al. reported a poly(tetrathiophene), i.e., PDCBT (Chart 1), which had two carboxylate substituents in each repeating unit. The HOMO energy level of this polymer was 0.36 eV lower than that of P3HT.[39] The fullerene-free PSCs based on PDCBT:ITIC with a high V_{oc} of 0.94 V and an excellent PCE of 10.16% were fabricated, while the device based on P3HT:ITIC showed a much lower V_{oc} of 0.52 V and a PCE of 1.25%.[43] To further enhance the V_{oc}, they attached F atoms to the backbone of PDCBT. The resulting polymer, PDCBT-2F (Chart 1), exhibited a deeper HOMO energy level of −5.56 eV, and a higher V_{oc} of 1.13 V with a PCE of 6.6% was achieved for PDCBT-2F:IT-M based device.[44] By use of the IT-4F acceptor, which has a lower LUMO energy level than IT-M, the device showed a high PCE over 11% with a decreased V_{oc} of 0.92 V.[45]

Fluorination has been a commonly used method for lowering HOMO and LUMO energy levels of multifarious organic semiconductors, including polymers and small molecules, in the past decade.[12,46−51] The F atom with a large Pauling electronegativity of 3.98[52] and a small van der Waals radius of 1.35 Å can lower the HOMO energy levels of polymers and avoid inducing a large steric effect. In addition, the molecular planarity could be improved through forming intramolecular F−S and F−H weak interactions. Compared to F, chlorine (Cl) is another electronegative halogen with smaller Pauling electronegativity (3.16).[52] Nevertheless, chlorinated polymers displayed even deeper HOMO energy levels than those of fluorinated polymers,[53−56] since the empty 3d-orbitals of the Cl atoms are available for π-electron delocalization, leading to increased electron density over the

DOI: 10.1021/acs.macromol.9b00793
Macromolecules 2019, 52, 4464−4474

Table 1. Number-Average Molecular Weights (M_n), Molar Mass Dispersities ($Đ$), and Photophysical and Electrochemical Parameters of the Polymers

			λ_{max} [nm]				
polymer	M_n [kDa]/$Đ$	$T_{d,5\%}$ [°C]	solution	film	E_g^{opt} [a] [eV]	E_{LUMO} [b]/E_{onset}^{re} [eV]	E_{HOMO} [b]/E_{onset}^{ox} [eV]
PDCBT	28.0/1.92	360	483	560/600	1.90	−2.90/−1.90	−5.20/0.40
PDCBT-F	24.7/2.13	392	501	533/594	1.93	−2.98/−1.82	−5.32/0.52
PDCBT-2F	22.4/2.20	372	501	511/592	1.92	−3.03/−1.77	−5.40/0.60
PDCBT-Cl	24.8/1.74	370	491	555/599	1.91	−3.01/−1.79	−5.34/0.54
PDCBT-2Cl	21.2/1.93	370	486	485/585	1.95	−3.00/−1.80	−5.44/0.64

[a]The optical bandgap E_g^{opt} was calculated from the film absorption onset. [b]The HOMO and LUMO energy levels were calculated according to $E_{HOMO} = -(4.80 + E_{onset}^{ox})$ eV and $E_{LUMO} = -(4.80 + E_{onset}^{re})$ eV, in which E_{onset}^{ox} and E_{onset}^{re} represent oxidation and reduction onset potentials, respectively, versus the half-potential of Fc/Fc^+.

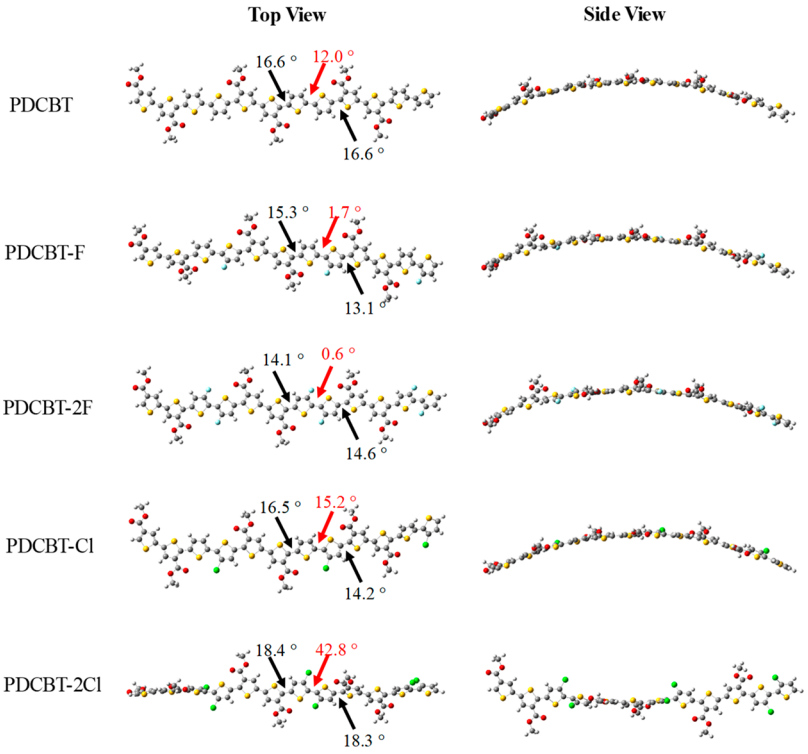

Figure 1. DFT optimized molecular geometries of the methyl-substituted trimers of the polymers.

Cl atoms relative to the F atoms.[57,58] More importantly, chlorinated polymers are much more accessible through convenient synthetic routes from commercial available chemicals in comparison to the corresponding fluorinated ones.[56] There have been several successful examples of chlorinated donor−acceptor conjugated polymers being applied in organic optoelectronic devices,[28,53−55,58−61] demonstrating that chlorination is a viable route toward developing high-performance materials.

Given that PTs have merits of ease synthesis and wide bandgap, the design, synthesis, and understanding of chlorinated PTs are important for the development of low-cost and high-performance polymer donor materials. In the current paper, we incorporated the Cl atoms to the backbone of PDCBT and designed and synthesized two chlorinated PTs with 3-chloro-2,2′-bithiophene (ClBT) and 3,3′-dichloro-2,2′-bithiophene (2ClBT) units, i.e., PDCBT-Cl and PDCBT-2Cl, as shown in Chart 1. For comparison, three polymers, i.e., PDCBT, PDCBT-F, and PDCBT-2F (Chart 1), with 2,2′-bithiophene (BT), 3-fluoro-2,2′-bithiophene (FBT), and 3,3′-difluoro-2,2′-bithiophene (2FBT) units, respectively, were also synthesized and characterized. The effects of the Cl substitution on the photophysical properties, film morphology, photovoltaic properties, and charge generation and recombination dynamics were investigated in detail. The PSC devices based on these polymers as donor materials and ITIC-Th1[62] (Chart 1), which has absorption spectrum complementary to these polymers, as acceptor material, were fabricated. The PDCBT-Cl based device yielded the highest PCE of 12.38% with a short-circuit current density (J_{sc}) of 18.50 mA cm^{-2}, a V_{oc} of 0.94 V, and a fill factor (FF) of 71.2%, while the devices with PDCBT, PDCBT-F, PDCBT-2F, and PDCBT-2Cl showed PCEs of 8.14%, 10.85%, 8.48%, and 6.94%, respectively.

RESULTS AND DISCUSSION

Materials Synthesis and Characterization. The synthesis of bis(2-hexyldecyl)-5,5′-dibromo-[2,2′-bithiophene]-4,4′-dicarboxylate (DCBT-2Br) monomer and the polymers is depicted in Scheme 1, and the details of the synthesis are described in the Supporting Information. Fluorinated and chlorinated thiophene monomers were prepared by following

DOI: 10.1021/acs.macromol.9b00793
Macromolecules 2019, 52, 4464−4474

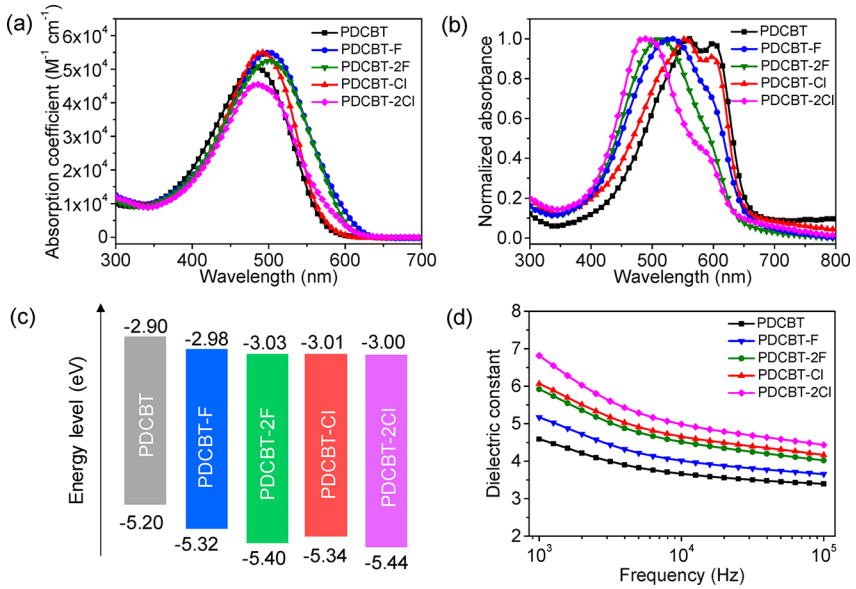

Figure 2. Solution (a, 10^{-5} mol/L in chloroform) and film (b) absorption spectra and schematic energy levels (c) of the polymers and the relative dielectric constants of the polymers at different frequencies (d).

the procedure reported in the literature.[47,60] The synthetic routes of chlorinated thiophene monomers delivered high reaction yields and are much shorter than those of fluorinated thiophene monomers. To realize the efficient preparation of the polymers, the synthesis of monomer DCBT-2Br was studied in detail. Route 1 was developed by Hou et al., and the monomer was obtained in three steps from compound **1**.[39] We found that the small amount of unknown impurities with polarity similar to the monomer was always present in the bromination step. Consequently, the repeated column chromatography purification was required to obtain the pure monomer. Because DCBT-2Br is a liquid, other purification techniques such as recrystallization cannot be used. These problems make the large-scale preparation of DCBT-2Br difficult. Then route 2 was developed. It is more efficient, and only two steps, including esterification and the direct arylation reaction, required from compound **4**, afforded the monomer in a two-step yield of 64%. Route 3 developed by Janssen et al. was also reinvestigated,[63] and the modified reaction conditions suitable to large-scale preparation were proposed. Via a typical esterification using methanol as reactant and solvent, the solid compound **6** was synthesized in a yield of 88% after recrystallization. Pd-catalyzed coupling of **6** afforded **7** in a yield of 85% after column chromatography and recrystallization. Because **8** is also a solid, trace amounts of impurities produced in bromination could be easily removed by recrystallization, giving compound **8** in a high yield (91%). Finally, the monomer DCBT-2Br was obtained via a transesterification. Because the reaction is clean and efficient (yield >90%), pure DCBT-2Br can be easily prepared on a several grams scale. However, this route is the longest among all three routes. Obviously, route 2 is the shortest and should be more suitable to the preparation of the monomer in large scale. All polymers were synthesized by typical Stille polycondensation in yields of 86%−95%. The chemical structures of the intermediates and the polymers were verified by NMR spectra (Figures S1−S9) and elemental analysis.

All the polymers exhibited good solubility in common chlorinated solvents, such as chloroform, chlorobenzene, and dichlorobenzene. The molecular weights of the polymers were determined by high-temperature gel permeation chromatography (GPC) at 150 °C using polystyrene as standard. The number-average molecular weights (M_n) of PDCBT, PDCBT-F, PDCBT-2F, PDCBT-Cl, and PDCBT-2Cl were 28.0, 24.7, 22.4, 24.8, and 21.2 kDa with corresponding molar mass dispersities ($Đ$) of 1.92, 2.13, 2.20, 1.74, and 1.93, respectively (Table 1). Similar molecular weights allow the fair comparison of the properties of the polymers. All five polymers exhibited good thermal stability with decomposition temperatures (T_d, 5% weight loss) exceeding 360 °C, as confirmed by thermogravimetric analysis (TGA) (Figure S10).

Density Functional Theory Calculations. Figure 1 depicts the optimized geometries of the trimers of the polymers by using the density functional theory (DFT) calculations at the B3LYP/6-31g(d) level. There was little difference of torsion angles (13°−18°) between carboxylate-substituted thiophene units and their adjacent thiophene units for these polymers. The torsion angles between the two thiophene rings in FBT (1.7°) and 2FBT (0.6°) units were much smaller than that in the BT (12.0°) unit. The improved coplanarity of the polymer backbones was induced by the presence of a weak intramolecular F−S interaction, as revealed by the smaller calculated F−S distances (2.94 Å for PDCBT-F and 2.92 Å for PDCBT-2F) than the sum of van der Waals radii of F and S atoms (3.27 Å). Different from the F atom, the Cl atom causes a less planar structure. The torsion angle between two thiophene units in ClBT (15.2°) was slightly higher than that in BT unit, whereas the torsion angle in 2ClBT unit with two Cl atoms sharply increased to 42.8°. The highly twisted conjugated backbone of PDCBT-2Cl could be detrimental for molecular packing. The calculated distribution of the frontier molecular orbitals of the trimers is shown in Figure S11. These polymers showed similar electron density distribution with HOMO and LUMO being delocalized over the whole conjugated backbone. The calculated HOMO/LUMO energy levels were −4.91/−2.59 eV for PDCBT-F, −5.10/−2.66 eV for PDCBT-2F, −5.00/−2.61 eV for PDCBT-Cl, and −5.32/−2.59 eV for PDCBT-2Cl, which are

DOI: 10.1021/acs.macromol.9b00793
Macromolecules 2019, 52, 4464−4474

lower than those (−4.87/−2.52 eV) of PDCBT because of the introduction of electron-withdrawing F and Cl atoms. Moreover, the F and Cl atoms preferentially stabilize the HOMO, resulting in the greater downshift of the HOMO energy levels than that of the LUMO energy levels.

Photophysical and Electrochemical Properties. The solution and film absorption spectra of the polymers are shown in Figure 2, and the corresponding data are summarized in Table 1. In solution, the five polymers showed similarly shaped absorption spectra with maxima at 483−501 nm (Figure 2a) and similar molar extinction coefficients, ranging from 4.5×10^4 to 5.5×10^4 L mol^{-1} cm^{-1} at maximum absorption peaks. From solution to film, the maximum absorption peaks were red-shifted by 77, 32, 10, and 64 nm for PDCBT, PDCBT-F, PDCBT-2F, and PDCBT-Cl, respectively, whereas PDCBT-2Cl showed an almost unchanged absorption maximum at 485 nm. In addition, a vibronic absorption shoulder peak appeared for all the five polymers at 585−600 nm, caused by intermolecular interactions in solid state. After thermal annealing at 150 °C, the shoulder peaks increased and became more pronounced for the polymers except PDCBT-2Cl whose shoulder was still weak with no obvious change (Figure S12). These results indicate the less effective intermolecular interaction of PDCBT-2Cl, which could be ascribed to the highly twisted conjugated backbones as predicted by DFT. The optical bandgaps of the polymers calculated from the film absorption onsets are 1.90, 1.93, 1.92, 1.91, and 1.95 eV for PDCBT, PDCBT-F, PDCBT-2F, PDCBT-Cl, and PDCBT-2Cl, respectively.

Thin film cyclic voltammograms (CV, see Figure S13) were measured to study the electrochemical properties of the five polymers. The HOMO and LUMO energy levels of the polymers were calculated from the redox onset potentials. As shown in Figure 2c and Table 1, the HOMO and LUMO energy levels are −5.20 and −2.90 eV for PDCBT, −5.32 and −2.98 eV for PDCBT-F, −5.40 and −3.03 eV for PDCBT-2F, −5.34 and −3.01 eV for PDCBT-Cl, and −5.44 and −3.00 eV for PDCBT-2Cl, respectively. Clearly, fluorination and chlorination endow the polymers with downshifted HOMO and LUMO energy levels, which is consistent with the DFT calculation results. In addition, the introduction of Cl atoms is more effective in terms of lowering HOMO energy levels of the polymers. This phenomenon is consistent with He's studies on donor−acceptor conjugated polymers.[54,55]

Dielectric Constant. The relative dielectric constants (ε_r) of the polymer neat films were determined by capacitance−voltage (C−V) measurements with a device architecture of ITO (indium tin oxide)/poly(3,4-ethylenedioxythiophene):poly(styrenesulfonate) (PEDOT:PSS, ∼ 30 nm)/polymer film (∼100 nm)/PDINO (10 nm, Figure S15)/Al (100 nm), where PDINO is an efficient cathode interlayer.[64] The relative dielectric constants were calculated by the equation of $\varepsilon_r = Cd/\varepsilon_0 A$, where C is the capacitance, d is the thickness of the polymer film, ε_0 is the vacuum dielectric constant, and A is the device area. The relative dielectric constants of the polymers as a function of frequency are shown in Figure 2d. The ε_r values at 10^4 Hz were 3.67, 4.01, 4.66, 4.52, and 4.99 for PDCBT, PDCBT-F, PDCBT-2F, PDCBT-Cl, and PDCBT-2Cl, respectively. Cleary, both fluorination and chlorination result in the enhanced ε_r, and the chlorinated polymers showed higher ε_r than their fluorinated counterparts. This is related to the polarity of the polymer backbones.[65−67] PDCBT:ITIC-Th1, PDCBT-F:ITIC-Th1, PDCBT-2F:ITIC-Th1, PDCBT-Cl:ITIC-Th1, and PDCBT-2Cl:ITIC-Th1 blend films showed ε_r of 2.47, 2.71, 2.98, 3.11, and 3.40, respectively (Figure S14). In PSCs, excitons should overcome the binding energy of the CT state (E_B^{CT}) to dissociate into free holes and electrons within the lifetime.[67,68] The E_B^{CT} estimated by the equation of $E_B^{CT} = q^2/(4\pi\varepsilon_0\varepsilon_r r_0)$,[69] where q is the elementary charge and r_0 is the electron and hole separation distance, were 0.39, 0.35, 0.32, 0.31, and 0.28 eV for PDCBT:ITIC-Th1, PDCBT-F:ITIC-Th1, PDCBT-2F:ITIC-Th1, PDCBT-Cl:ITIC-Th1, and PDCBT-2Cl:ITIC-Th1 blend films, respectively. The lower E_B^{CT} of the blend films based on the fluorinated and chlorinated polymers would be beneficial for charge separation in PSCs.

Molecular Packing and Hole Transport Properties. Two-dimensional grazing-incidence wide-angle X-ray scattering (2D-GIWAXS) was used to investigate the molecular packing and orientation of the polymers in neat films. The GIWAXS patterns and the corresponding profiles of the polymers are shown in Figure S16, and the crystalline coherence lengths (CCLs) of the polymers are summarized in Table S1. PDCBT neat films showed a pronounced (100) diffraction peak at 0.29 Å^{-1} in the out-of-plane (q_z) direction, corresponding to a d-spacing of 21.7 Å, and a (010) diffraction located at ∼1.72 Å^{-1} in the in-plane (q_{xy}) direction stronger than that in the q_z direction, corresponding to a π−π stacking distance of ∼3.65 Å. The PDCBT-F, PDCBT-2F, and PDCBT-Cl neat films presented clear (100) diffractions in both q_{xy} and q_z directions, with lamellar packing d-spacing of 23.4−26.1 Å. The (010) diffraction peaks were located at ∼1.72 Å^{-1} in the q_z direction with d-spacings of ∼3.65 Å, identical to that of PDCBT, while no discernible (010) diffraction was observed in the q_{xy} direction. These results indicate that PDCBT backbones tend to form an edge-on orientation, but PDCBT-F, PDCBT-2F, and PDCBT-Cl exhibit more preferential face-on molecular packing. In addition, the (010) CCLs of PDCBT-F, PDCBT-2F, and PDCBT-Cl films were 44.9, 43.7, and 46.5 Å (in the q_z direction), respectively, which were longer than that of PDCBT (39.7 Å (in the q_{xy} direction)). The ordered face-on π−π stacking is desirable for photovoltaic devices, which is favorable to the charge transport in vertical sandwich device architecture. For PDCBT-2Cl neat film, (100) and (200) diffraction peaks existed in the q_z direction with a lamellar d-spacing of 24.4 Å, and extremely weak (010) diffraction peaks were observed in q_{xy} and q_z directions with a d-spacing of ∼3.74 Å larger than those of other four polymers (∼3.65 Å). The poor intermolecular π−π stacking with short CCLs (34.3 Å in q_{xy}) and the large π−π stacking distance of PDCBT-2Cl could be ascribed to the severe distortion of the backbones. Compared with PDCBT (lamellar d-spacing: ∼21.7 Å), PDCBT-F, PDCBT-2F, PDCBT-Cl, and PDCBT-2Cl displayed slightly larger lamellar d-spacings (23.4−26.1 Å), which could be attributed to the larger radii of F and Cl atoms relative to that of H atom and therefore larger space for the interdigitation of side chains. The microstructure of ITIC-Th1 neat film was also characterized by in-plane and out-of-plane XRD. As shown in Figure S17, ITIC-Th1 backbones are prone to form face-on orientation. The obvious (100) and (010) diffraction peaks at $2\theta = 6.5°$ and $2\theta = 25.8°$, corresponding to d-spacings of 13.6 and 3.5 Å, respectively, were observed in the out-of-plane direction, while there was no obvious peak in the in-plane direction.

DOI: 10.1021/acs.macromol.9b00793
Macromolecules 2019, 52, 4464−4474

The hole transport property of the polymers was investigated by the space-charge limited current (SCLC) method with a device architecture of ITO/PEDOT:PSS (~30 nm)/polymer film (~100 nm)/Au (100 nm), as shown in Figure S18 and Table S2. Compared to PDCBT with a hole mobility (μ_h) of 0.65×10^{-4} cm^2 V^{-1} s^{-1}, PDCBT-F, PDCBT-Cl, and PDCBT-2F exhibited somewhat higher μ_h of 0.82×10^{-4}, 0.84×10^{-4}, and 0.79×10^{-4} cm^2 V^{-1} s^{-1}, respectively, benefiting from the ordered face-on backbone packing in the films. Owing to the poor molecular $\pi-\pi$ stacking, PDCBT-2Cl showed the lowest μ_h of 0.49×10^{-4} cm^2 V^{-1} s^{-1}.

Photovoltaic Properties. To evaluate the photovoltaic performance of these polymers, PSC devices with an architecture of ITO/PEDOT:PSS (~30 nm)/polymer:ITIC-Th1/PDINO (~10 nm)/Al (100 nm) were fabricated. The typical current density−voltage ($J-V$) curves are displayed in Figure 3a, and the corresponding device parameters are summarized in Table 2. The device fabrication conditions of the PSCs were systematically screened by varying the D/A ratios, active layer thickness, and post-treatments (see Tables S3−S7). The optimized devices were fabricated by using chloroform as the processing solvent with a donor/acceptor weight ratio of 1:1 and an active-layer thickness of ~110 nm. Without any post-treatment, PSCs based on PDCBT, PDCBT-F, PDCBT-2F, PDCBT-Cl, and PDCBT-2Cl showed PCEs of 6.44%, 8.37%, 7.32%, 8.05%, and 5.94%, respectively. The V_{oc}s of these devices follow the order of PDCBT < PDCBT-F, PDCBT-Cl < PDCBT-2F, PDCBT-2Cl, which is consistent with the lower HOMO energy levels induced by fluorination and chlorination in PDCBT series. In addition, the PDCBT-F, PDCBT-2F, PDCBT-Cl, and PDCBT-2Cl based devices displayed reduced E_{loss} with the values of 0.60, 0.56, 0.60, and 0.55 eV, respectively, compared with PDCBT based device (E_{loss} = 0.66 eV). The J_{sc}s and FFs were improved after thermal annealing (TA) and solvent vapor annealing (SVA) for all polymers. With the 100 °C TA treatment, the PCEs of the PSCs based on PDCBT, PDCBT-F, PDCBT-2F, PDCBT-Cl, and PDCBT-2Cl were enhanced to 7.06%, 9.76%, 7.63%, 10.16%, and 6.41%, respectively. Upon SVA treatment with carbon disulfide (CS_2) for 120 s, all polymers achieved the best device performance with higher J_{sc}s and FFs relative to their counterparts with TA treatment. The device based on PDCBT showed a PCE of 8.14% with aV_{oc} of 0.89 V, aJ_{sc} of 16.60 mA cm^{-2}, and aFF of 55.2%. The devices based on PDCBT-F and PDCBT-Cl exhibited superior V_{oc}s, J_{sc}s, and FFs, thus high PCEs exceeding 10%. A PCE of 12.38% with a V_{oc} of 0.94 V, a J_{sc} of 18.50 mA cm^{-2}, and a FF of 71.2% was achieved for PDCBT-Cl, which is the best photovoltaic performance for polythiophene derivatives reported so far. The PDCBT-2F and PDCBT-2Cl based devices afforded significantly elevated V_{oc}s, but relatively low J_{sc}s and FFs, leading to inferior PCEs of 8.48% and 6.94%, respectively, relative to their monosubstituted counterparts. Figure 3b shows the external quantum efficiency (EQE) curves of the optimized devices. All the PSC devices displayed broad response from 300 to 820 nm. Compared with the devices based on PDCBT, PDCBT-F, and PDCBT-2F, the PDCBT-Cl based device gave much higher EQE exceeding 70% in a broad wavelength range from 450 to 700 nm, while the PDCBT-2Cl based device showed relatively lower EQE. The calculated J_{sc}s obtained from EQE curves were in accordance with those extracted from $J-V$ curves within an acceptable deviation of 5%. The charge transport properties of the blend films were examined by using the SCLC method, and the corresponding data are shown in Figure S19 and Table S8. The μ_h and electron mobility (μ_e) of all the blend films with TA and SVA treatments were higher than their counterparts without any post-treatment, and the

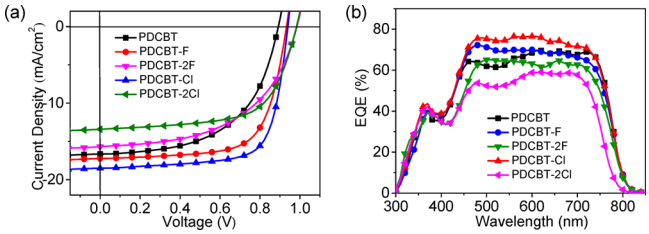

Figure 3. Current density−voltage ($J-V$) characteristics (a) and the external quantum efficiency (EQE) curves (b) of the PSCs under the optimized conditions.

Table 2. Photovoltaic Performance of the PSCs Based on the Polymers under Different Conditions

polymer	treatment[a]	J_{sc}[b] (mA/cm^2)	V_{oc}[b] (V)	FF[b] (%)	PCE[b] (%)
PDCBT	as cast	13.02 ± 0.25 (13.33)	0.91 ± 0.01 (0.92)	44.2 ± 1.0 (45.8)	6.23 ± 0.17 (6.44)
	TA	15.65 ± 0.20 (15.92)	0.90 ± 0.01 (0.90)	47.6 ± 1.0 (49.2)	6.79 ± 0.21 (7.06)
	SVA	16.35 ± 0.21 (16.60)	0.88 ± 0.01 (0.89)	53.8 ± 0.9 (55.2)	7.86 ± 0.22 (8.14)
PDCBT-F	as cast	13.96 ± 0.15 (14.15)	0.95 ± 0.01 (0.95)	60.1 ± 1.2 (61.8)	8.06 ± 0.25 (8.37)
	TA	16.51 ± 0.19 (16.75)	0.94 ± 0.01 (0.94)	60.7 ± 0.8 (62.0)	9.47 ± 0.22 (9.76)
	SVA	17.27 ± 0.20 (17.52)	0.93 ± 0.01 (0.93)	64.9 ± 1.0 (66.2)	10.54 ± 0.23 (10.85)
PDCBT-2F	as cast	13.49 ± 0.20 (13.73)	0.98 ± 0.01 (0.99)	52.0 ± 1.2 (53.8)	7.03 ± 0.24 (7.32)
	TA	14.13 ± 0.25 (14.44)	0.97 ± 0.01 (0.98)	52.5 ± 0.9 (54.0)	7.35 ± 0.20 (7.63)
	SVA	15.03 ± 0.23 (15.32)	0.98 ± 0.01 (0.98)	55.1 ± 1.1 (56.5)	8.23 ± 0.18 (8.48)
PDCBT-Cl	as cast	14.05 ± 0.21 (14.34)	0.94 ± 0.01 (0.95)	57.9 ± 0.8 (59.1)	7.79 ± 0.20 (8.05)
	TA	17.15 ± 0.19 (17.40)	0.93 ± 0.01 (0.94)	60.1 ± 1.3 (62.1)	9.87 ± 0.22 (10.16)
	SVA	18.28 ± 0.18 (18.50)	0.93 ± 0.01 (0.94)	69.6 ± 1.1 (71.2)	12.11 ± 0.19 (12.38)
PDCBT-2Cl	as cast	12.84 ± 0.17 (13.06)	1.00 ± 0.01 (1.00)	44.1 ± 0.9 (45.5)	5.64 ± 0.23 (5.94)
	TA	13.08 ± 0.20 (13.35)	0.98 ± 0.01 (0.99)	46.7 ± 1.1 (48.5)	6.13 ± 0.20 (6.41)
	SVA	13.26 ± 0.22 (13.54)	0.98 ± 0.01 (0.99)	50.2 ± 1.0 (51.8)	6.65 ± 0.21 (6.94)

[a]The TA treatment was conducted at 100 °C for 10 min, and the SVA treatment was conducted with CS_2 for 120 s. [b]Statistical and optimal results are listed outside of parentheses and in parentheses, respectively. The average values are obtained from over 15 devices. TA: thermal annealing; SVA: solvent vapor annealing.

DOI: 10.1021/acs.macromol.9b00793
Macromolecules 2019, 52, 4464−4474

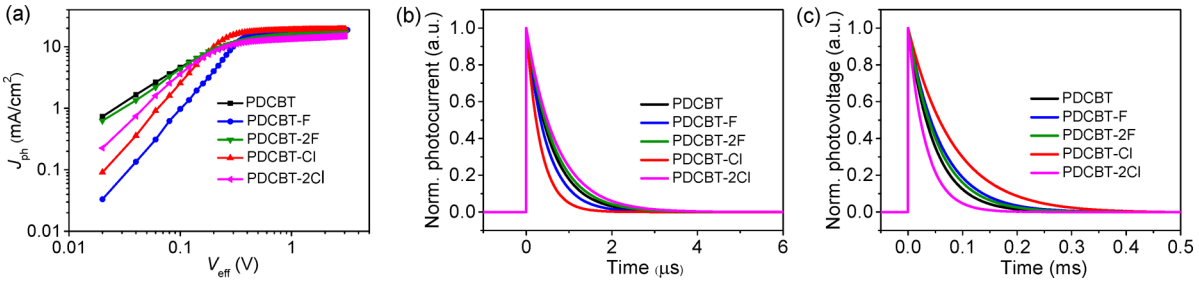

Figure 4. Photocurrent density versus effective voltage ($J_{ph} - V_{eff}$) characteristics (a), transient photocurrent (b), and transient photovoltage (c) measurements for the PSCs under the optimized conditions.

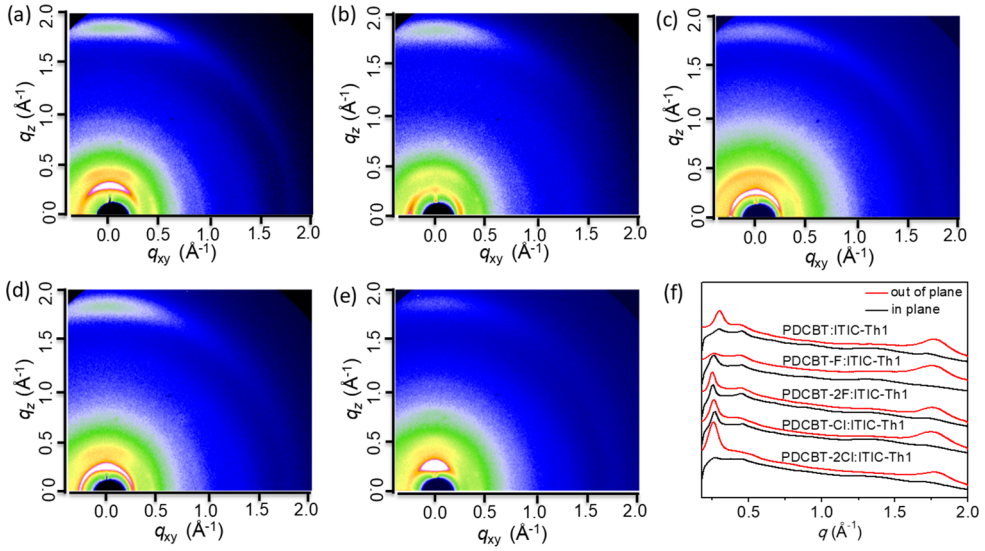

Figure 5. 2D-GIWAXS patterns for PDCBT:ITIC-Th1 (a), PDCBT-F:ITIC-Th1 (b), PDCBT-2F:ITIC-Th1 (c), PDCBT-Cl:ITIC-Th1 (d), and PDCBT-2Cl:ITIC-Th1 (e) blend films with SVA treatment and the out-of-plane and in-plane GIWAXS profiles for the blend films (f) derived from (a–e).

highest charge mobility was obtained by SVA treatment for all the blends. With SVA treatment, μ_h and μ_e were 0.95×10^{-4} and 0.31×10^{-4} cm^2 V^{-1} s^{-1} for PDCBT:ITIC-Th1, 1.15×10^{-4} and 0.47×10^{-4} cm^2 V^{-1} s^{-1} for PDCBT-F:ITIC-Th1, 0.96×10^{-4} and 0.35×10^{-4} cm^2 V^{-1} s^{-1} for PDCBT-2F:ITIC-Th1, 1.53×10^{-4} and 0.71×10^{-4} cm^2 V^{-1} s^{-1} for PDCBT-Cl:ITIC-Th1, and 0.63×10^{-4} and 0.20×10^{-4} cm^2 V^{-1} s^{-1} for PDCBT-2Cl:ITIC-Th1, respectively. The PDCBT-2Cl:ITIC-Th1 blend film exhibited the inferior charge mobility, which could be ascribed to the weak $\pi-\pi$ stacking of PDCBT-2Cl backbones and the unfavorable morphology as discussed below. The high hole and electron mobilities of PDCBT-Cl:ITIC-Th1 blend film are the key factors for the high J_{sc} and FF of the PSCs.

To investigate charge generation and extraction involved in the PSC devices, the effective voltage (V_{eff}) dependent photocurrent density (J_{ph}) was measured (Figure 4a). As shown in Figure 4a, J_{ph} for all devices increased with V_{eff} and reached a saturated value (saturation current density, J_{sat}) at high V_{eff}. The overall exciton dissociation probability can be estimated from the ratio of J_{ph}/J_{sat}. At the short-circuit conditions, the ratios of J_{ph}/J_{sat} were 90%, 93%, 91%, 96%, and 88% for the devices based on PDCBT, PDCBT-F, PDCBT-2F, PDCBT-Cl, and PDCBT-2Cl, respectively. At the maximal power output conditions, the ratios for PDCBT, PDCBT-F, PDCBT-2F, PDCBT-Cl, and PDCBT-2Cl based devices were 83%, 90%, 86%, 92%, and 79%, respectively. The high J_{ph}/J_{sat} ratios of PDCBT-Cl based device are indicative of efficient process of exciton dissociation and charge collection. This could be a result of the ordered molecular packing and the desirable blend film morphology as discussed below, and the low E_B^{CT} in the PDCBT-Cl:ITIC-Th1 blend film might also contribute to the efficient exciton dissociation.[66,70] For the PDCBT-2Cl:ITIC-Th1 blend film, which also had a low E_B^{CT}, the inefficient exciton dissociation in the device should have resulted from the severe phase separation in the film, as revealed in the Film Microstructures and Morphology section. Figures 4b and 4c showed transient photocurrent and photovoltage decay kinetics of the optimized devices based on the polymers. The charge sweep-out time at short-circuit condition was 0.58 μs for the PDCBT based device, 0.42 μs for the PDCBT-F based device, 0.62 μs for the PDCBT-2F based device, 0.35 μs for the PDCBT-Cl based device, and 0.72 μs for the PDCBT-2Cl based device. The difference in the sweep-out time can be correlated to the charge mobility in the blend films. For example, the higher charge mobility in the PDCBT-Cl:ITIC-Th1 blend film is responsible for the shorter charge extraction time. The carrier lifetimes calculated from the traces of transient photovoltage (TPV) measurements were 57, 62, 51, 83, and 35 μs for the devices based on PDCBT, PDCBT-F, PDCBT-2F, PDCBT-Cl, and PDCBT-2Cl, respectively.[71,72] The lifetime of carriers at open-circuit voltage is dominated by recombination. The much longer carrier lifetime in the PDCBT-Cl based device may indicate less recombination,

DOI: 10.1021/acs.macromol.9b00793
Macromolecules 2019, 52, 4464–4474

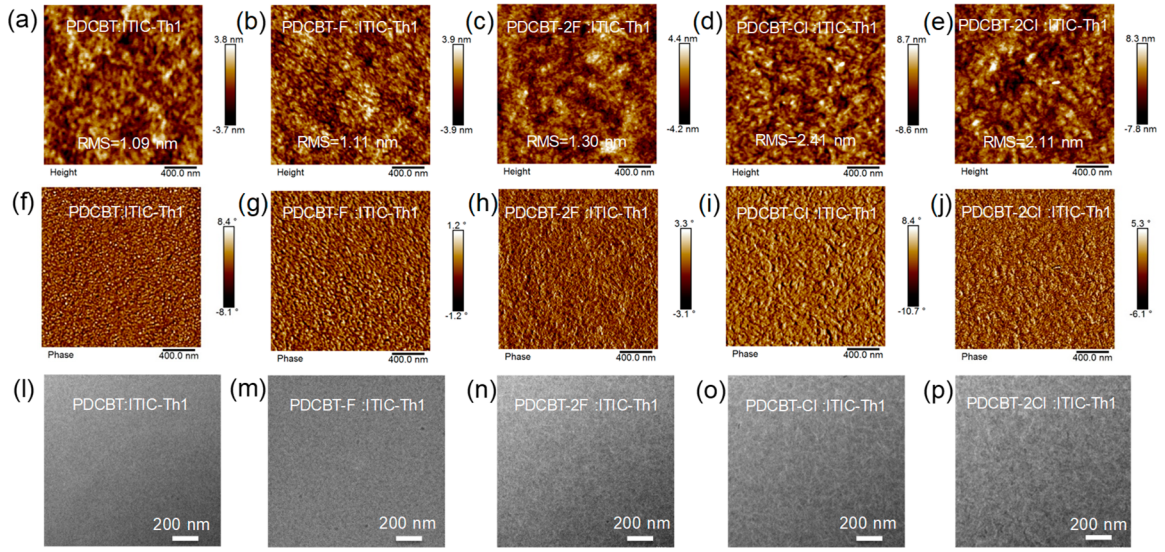

Figure 6. AFM height (a–e) and phase (f–j) images and TEM images (l–p) of polymer:ITIC-Th1 blend films with SVA treatment.

Table 3. Contact Angle, Surface Tension of Individual Materials, and $(\sqrt{\gamma_{donor}} - \sqrt{\gamma_{acceptor}})^2$ Values

organic layer X	contact angle [water] (deg)	contact angle [GL] (deg)	γ^d (mN/m)	γ^p (mN/m)	surface tension (mN/m)	$(\sqrt{\gamma_{donor}} - \sqrt{\gamma_{acceptor}})^2$
ITIC-Th1	100.39	85.80	22.36	4.20	26.56	
PDCBT	104.87	91.30	20.50	3.15	23.65	0.07
PDCBT-F	105.24	91.98	19.91	3.20	23.11	0.11
PDCBT-2F	106.19	93.51	18.83	3.21	22.04	0.20
PDCBT-Cl	105.80	93.89	17.04	4.23	21.27	0.27
PDCBT-2Cl	105.33	94.17	16.12	4.48	20.60	0.35

which is consistent to the superior J_{sc} and FF. Nevertheless, the long charge extraction time and short carrier lifetime for PDCBT-2Cl based device agree with its low photovoltaic performance.

Film Microstructures and Morphology. The molecular packing in the blend films with different treatments was studied by 2D-GIWAXS. Compared to the untreated blend films (Figure S20), the blend films with TA (Figure S21) or SVA (Figure 5) treatment showed improved crystallinity, as indicated by the stronger diffraction peaks with larger CCLs (Table S9) in both q_{xy} and q_z directions. In the blend films with SVA treatment, the (100) diffraction peaks arising from lamellar packing of the polymers were observed in q_{xy} and q_z directions at 0.30 $Å^{-1}$ for PDCBT:ITIC-Th1 and 0.25–0.27 $Å^{-1}$ for the other four blend films, corresponding to d-spacings of 20.9 and 25.1–23.3 Å, respectively. The larger lamellar d-spacing of PDCBT-F, PDCBT-2F, PDCBT-Cl, and PDCBT-2Cl than that of PDCBT in the blend films is in accordance with the 2D-GIWAXS data in the neat polymer films. The (100) peaks at ~0.45 $Å^{-1}$ with a d-spacing of ~13.9 Å coming from ITIC-Th1 existed in all the SVA-treated blend films. The (100) diffraction from ITIC-Th1 in the PDCBT-2Cl:ITIC-Th1 blend film was only observed in the q_{xy} direction, and the CCL (62.4 Å) was shorter than those in the other blend films (85.2–87.6 Å in q_{xy}, 82.4–84.9 Å in q_z), implying the poor lamellar packing of ITIC-Th1. All the blend films showed more intense (010) diffraction peaks at 1.76–1.79 $Å^{-1}$ in the q_z direction than those in the q_{xy} direction. The broad (010) peaks could be ascribed to the overlapped diffractions of the polymers and ITIC-Th1. The (010) diffraction peaks in PDCBT-F:ITIC-Th1 and PDCBT-Cl:ITIC-Th1 blend films were more intense with CCLs of 33.9 and 34.9 Å in the q_z direction, respectively, which were larger than those in PDCBT:ITIC-Th1 (28.8 Å), PDCBT-2F:ITIC-Th (31.0 Å), and PDCBT-2Cl:ITIC-Th (28.5 Å) films. The more ordered π–π stacking in PDCBT-F:ITIC-Th1 and PDCBT-Cl:ITIC-Th1 films is a benefit for charge transport in the PSCs. The PDCBT-2Cl:ITIC-Th1 blend film presented the relatively weak (010) diffraction peak with the shortest CCL in comparison to other blend films. This indicates poor π–π stacking between the molecules, resulting in the low charge carrier mobility.

To comprehensively understand the different device performance of these polymers, the morphology of the blend films was investigated by atomic force microscopy (AFM) and transmission electron microscopy (TEM). The AFM images of the blend films with different treatments are shown in Figures S22 and S23 as well as Figure 6a–j, and all blend films were smooth and uniform. Without any post-treatment, the blend films showed a root-mean-square (rms) roughness from 0.61 to 1.55 nm. After TA or SVA treatment, the rms roughness slightly increased to 1–3 nm. From AFM phase images, all blend films exhibited more pronounced phase separation after TA and SVA treatments. The TEM images of the blend films with SVA treatment are displayed in Figure 6l–p. The nanoscale phase separation with different domain sizes was observed for all blend films, in accordance with AFM results. There was no obvious phase separation of the donor and the acceptor in the PDCBT:ITIC-Th1 blend film, which could obstruct charge transport. In contrast, the blend films based on fluorinated and chlorinated polymers exhibited more pronounced phase separation, likely due to the reduced miscibility

DOI: 10.1021/acs.macromol.9b00793
Macromolecules 2019, 52, 4464–4474

between the fluorinated/chlorinated polymers and ITIC-Th1, as discussed below. Nevertheless, relatively large aggregates were observed in the PDCBT-2Cl:ITIC-Th1 blend film, which could induce unfavorable exciton recombination and hence reduced charge generation. The PDCBT-Cl:ITIC-Th1 blend film exhibited more desirable morphology with polymer-rich fibrils of hundreds of nanometers in length and several nanometers in width close to the exciton diffusion length in organic materials. The well-percolated bicontinuous network of the PDCBT-Cl:ITIC-Th1 blend film is highly favorable for charge generation and transport, consistent with the aforementioned device results.

The miscibility of the donor and acceptor materials has a great influence on the blend film morphology. To further understand the molecular miscibility between these polymer donors and ITIC-Th1, we measured the contact angles of the neat films based on the polymers and ITIC-Th1 and calculated their surface tension (γ) (Figure S24 and Table 3). The surface tensions of all polymer films (20.60−23.65 mN/m) are lower than that (26.56 mN/m) of the ITIC-Th1 film. In addition, the polymers with F or Cl substituents, i.e., PDCBT-F, PDCBT-2F, PDCBT-Cl, and PDCBT-2Cl, showed reduced surface tension with values of 23.11, 22.04, 21.27, and 20.60 mN/m, respectively, compared to that (23.65 mN/m) of PDCBT; the chlorinated polymers (PDCBT-Cl and PDCBT-2Cl) showed lower surface tension than those of the fluorinated polymers (PDCBT-F and PDCBT-2F). The molecular interaction parameter $\chi \propto (\sqrt{\gamma_{\text{donor}}} - \sqrt{\gamma_{\text{acceptor}}})^2$ suggested by Moons and co-workers, in which χ is the Flory−Huggins interaction parameter, was used to compare the miscibility of the polymer donor and acceptor materials in the blend.[26,73,74] The smaller χ or $(\sqrt{\gamma_{\text{donor}}} - \sqrt{\gamma_{\text{acceptor}}})^2$ values imply a higher degree of molecular miscibility between the two materials. According to the $(\sqrt{\gamma_{\text{donor}}} - \sqrt{\gamma_{\text{acceptor}}})^2$ values in Table 3, the molecular miscibility of the polymers and ITIC-Th1 follows the order of PDCBT > PDCBT-F > PDCBT-2F > PDCBT-Cl > PDCBT-2Cl. The lack of obvious phase separation in the PDCBT:ITIC-Th1 blend film could be caused by the high molecular intermixing between PDCBT and ITIC-Th1. The poor miscibility of PDCBT-2Cl and ITIC-Th1 should be a reason for the severe phase separation of the polymer donor and the acceptor in the blend film. The suitable molecular miscibility of PDCBT-F:ITIC-Th1, PDCBT-2F:ITIC-Th1, and PDCBT-Cl:ITIC-Th1 systems contributes to the more appropriate phase separation in the blend films.

CONCLUSIONS

In summary, we have synthesized five polythiophene derivatives, i.e., PDCBT, PDCBT-F, PDCBT-Cl, PDCBT-2,F and PDCBT-2Cl, with wide optical bandgaps of 1.90−1.95 eV. The effects of the chlorination on photophysical and charge transport properties, molecular packing, and film microstructures were studied comprehensively in comparison to the fluorination. The chlorinated and fluorinated polymers possess deeper HOMO and LUMO energy levels and higher dielectric constants than their unsubstituted counterpart PDCBT. As expected from the deep HOMO energy levels, PDCBT-F and PDCBT-Cl based PSCs showed enhanced V_{oc} of 0.93 V, and the V_{oc} of PDCBT-2F and PDCBT-2Cl based PSCs reached 0.98 V, higher than that of PDCBT based PSCs (V_{oc} = 0.89 V). Compared to PDCBT and the fluorinated polymers (PDCBT-F and PDCBT-2F), PDCBT-Cl with monochlorinated BT unit had a higher hole mobility, while PDCBT-2Cl with dichlorinated BT displayed a lower hole mobility due to the poor intermolecular $\pi-\pi$ stacking derived from the highly twisted backbone. The PDCBT-Cl:ITIC-Th1 blend film showed a proper phase-separated morphology with favorable molecular packing and miscibility, resulting in the efficient exciton dissociation and charge collection as well as weak recombination in the PSC device. Consequently, the PDCBT-Cl:ITIC-Th1 based PSCs achieved the highest PCE of 12.38% with a V_{oc} of 0.94 V, a J_{sc} of 18.50 mA cm^{-2}, and a FF of 71.2%, which is the best photovoltaic performance for polythiophene derivatives reported so far. Owing to the structural simplicity and synthetic accessibility of the monomers, the high-performance chlorinated polythiophene PDCBT-Cl is promising for future PSC commercialization.

ASSOCIATED CONTENT

Supporting Information

The Supporting Information is available free of charge on the ACS Publications website at DOI: 10.1021/acs.macromol.9b00793.

Details of synthesis of monomers and polymers, instruments, device fabrication and characterization, SCLC measurements, 2D-GIWAXS data, AFM and TEM images, and other data (PDF)

AUTHOR INFORMATION

Corresponding Authors

*E-mail miaomiao.li@tju.edu.cn; m.li4@tue.nl.
*E-mail yanhou.geng@tju.edu.cn.

ORCID

Jianhui Hou: 0000-0002-2105-6922
René A. J. Janssen: 0000-0002-1920-5124
Yanhou Geng: 0000-0002-4997-3925

Notes

The authors declare no competing financial interest.

ACKNOWLEDGMENTS

This work is supported by the National Natural Science Foundation of China (No. 21574128 and 51703158). The research also received funding from the European Research Council (ERC Grant Agreement No. 33903). The authors thank the Beijing Synchrotron Radiation Facility (BSRF) for the help with 2D GIWAXS measurements.

REFERENCES

(1) He, Z.; Xiao, B.; Liu, F.; Wu, H.; Yang, Y.; Xiao, S.; Wang, C.; Russell, T. P.; Cao, Y. Single-junction polymer solar cells with high efficiency and photovoltage. *Nat. Photonics* **2015**, *9*, 174−179.

(2) Li, G.; Zhu, R.; Yang, Y. Polymer solar cells. *Nat. Photonics* **2012**, *6*, 153−161.

(3) Yu, G.; Gao, J.; Hummelen, J. C.; Wudl, F.; Heeger, A. J. J. S. Polymer Photovoltaic Cells: Enhanced Efficiencies via a Network of Internal Donor-Acceptor Heterojunctions. *Science* **1995**, *270*, 1789−1791.

(4) Cheng, P.; Li, G.; Zhan, X.; Yang, Y. Next-generation organic photovoltaics based on non-fullerene acceptors. *Nat. Photonics* **2018**, *12*, 131−142.

(5) Gao, G.; Liang, N.; Geng, H.; Jiang, W.; Fu, H.; Feng, J.; Hou, J.; Feng, X.; Wang, Z. Spiro-Fused Perylene Diimide Arrays. *J. Am. Chem. Soc.* **2017**, *139*, 15914−15920.

DOI: 10.1021/acs.macromol.9b00793
Macromolecules 2019, 52, 4464−4474

(6) Gao, L.; Zhang, Z. G.; Xue, L.; Min, J.; Zhang, J.; Wei, Z.; Li, Y. All-Polymer Solar Cells Based on Absorption-Complementary Polymer Donor and Acceptor with High Power Conversion Efficiency of 8.27%. *Adv. Mater.* **2016**, *28*, 1884−1890.
(7) Hou, J.; Inganas, O.; Friend, R. H.; Gao, F. Organic solar cells based on non-fullerene acceptors. *Nat. Mater.* **2018**, *17*, 119−128.
(8) Lin, Y.; Wang, J.; Zhang, Z. G.; Bai, H.; Li, Y.; Zhu, D.; Zhan, X. An electron acceptor challenging fullerenes for efficient polymer solar cells. *Adv. Mater.* **2015**, *27*, 1170−1174.
(9) Meng, D.; Sun, D.; Zhong, C.; Liu, T.; Fan, B.; Huo, L.; Li, Y.; Jiang, W.; Choi, H.; Kim, T.; Kim, J. Y.; Sun, Y.; Wang, Z.; Heeger, A. J. High-Performance Solution-Processed Non-Fullerene Organic Solar Cells Based on Selenophene-Containing Perylene Bisimide Acceptor. *J. Am. Chem. Soc.* **2016**, *138*, 375−380.
(10) Yan, C.; Barlow, S.; Wang, Z.; Yan, H.; Jen, A. K. Y.; Marder, S. R.; Zhan, X. Non-fullerene acceptors for organic solar cells. *Nat. Rev. Mater.* **2018**, *3*, 18003.
(11) Yuan, J.; Huang, T.; Cheng, P.; Zou, Y.; Zhang, H.; Yang, J. L.; Chang, S. Y.; Zhang, Z.; Huang, W.; Wang, R.; Meng, D.; Gao, F.; Yang, Y. Enabling low voltage losses and high photocurrent in fullerene-free organic photovoltaics. *Nat. Commun.* **2019**, *10*, 570−578.
(12) Cui, Y.; Yang, C.; Yao, H.; Zhu, J.; Wang, Y.; Jia, G.; Gao, F.; Hou, J. Efficient Semitransparent Organic Solar Cells with Tunable Color enabled by an Ultralow-Bandgap Nonfullerene Acceptor. *Adv. Mater.* **2017**, *29*, 1703080.
(13) Li, T.; Dai, S.; Ke, Z.; Yang, L.; Wang, J.; Yan, C.; Ma, W.; Zhan, X. Fused Tris(thienothiophene)-Based Electron Acceptor with Strong Near-Infrared Absorption for High-Performance As-Cast Solar Cells. *Adv. Mater.* **2018**, *30*, 1705969.
(14) Li, Y.; Zhong, L.; Gautam, B.; Bin, H.-J.; Lin, J.-D.; Wu, F.-P.; Zhang, Z.; Jiang, Z.-Q.; Zhang, Z.-G.; Gundogdu, K.; Li, Y.; Liao, L.-S. A near-infrared non-fullerene electron acceptor for high performance polymer solar cells. *Energy Environ. Sci.* **2017**, *10*, 1610−1620.
(15) Liu, F.; Zhou, Z.; Zhang, C.; Zhang, J.; Hu, Q.; Vergote, T.; Liu, F.; Russell, T. P.; Zhu, X. Efficient Semitransparent Solar Cells with High NIR Responsiveness Enabled by a Small-Bandgap Electron Acceptor. *Adv. Mater.* **2017**, *29*, 1606574.
(16) Shi, X.; Liao, X.; Gao, K.; Zuo, L.; Chen, J.; Zhao, J.; Liu, F.; Chen, Y.; Jen, A. K. Y. An Electron Acceptor with Broad Visible-NIR Absorption and Unique Solid State Packing for As-Cast High Performance Binary Organic Solar Cells. *Adv. Funct. Mater.* **2018**, *28*, 1802324.
(17) Shi, X.; Zuo, L.; Jo, S. B.; Gao, K.; Lin, F.; Liu, F.; Jen, A. K. Y. Design of a Highly Crystalline Low-Band Gap Fused-Ring Electron Acceptor for High-Efficiency Solar Cells with Low Energy Loss. *Chem. Mater.* **2017**, *29*, 8369−8376.
(18) Wang, W.; Yan, C.; Lau, T. K.; Wang, J.; Liu, K.; Fan, Y.; Lu, X.; Zhan, X. Fused Hexacyclic Nonfullerene Acceptor with Strong Near-Infrared Absorption for Semitransparent Organic Solar Cells with 9.77% Efficiency. *Adv. Mater.* **2017**, *29*, 1701308.
(19) Xiao, Z.; Jia, X.; Ding, L. Ternary organic solar cells offer 14% power conversion efficiency. *Sci. Bull.* **2017**, *62*, 1562−1564.
(20) Yao, H.; Cui, Y.; Yu, R.; Gao, B.; Zhang, H.; Hou, J. Design, Synthesis, and Photovoltaic Characterization of a Small Molecular Acceptor with an Ultra-Narrow Band Gap. *Angew. Chem., Int. Ed.* **2017**, *56*, 3045−3049.
(21) Liang, Z.; Li, M.; Zhang, X.; Wang, Q.; Jiang, Y.; Tian, H.; Geng, Y. Near-infrared absorbing non-fullerene acceptors with selenophene as π bridges for efficient organic solar cells. *J. Mater. Chem. A* **2018**, *6*, 8059−8067.
(22) Cui, Y.; Yao, H.; Hong, L.; Zhang, T.; Xu, Y.; Xian, K.; Gao, B.; Qin, J.; Zhang, J.; Wei, Z.; Hou, J. Achieving Over 15% Efficiency in Organic Photovoltaic Cells via Copolymer Design. *Adv. Mater.* **2019**, *31*, 1808356.
(23) Fan, B.; Zhang, D.; Li, M.; Zhong, W.; Zeng, Z.; Ying, L.; Huang, F.; Cao, Y. Achieving over 16% efficiency for single-junction organic solar cells. *Sci. China: Chem.* **2019**, DOI: 10.1007/s11426-019-9457-5.
(24) Geng, R.; Song, X.; Feng, H.; Yu, J.; Zhang, M.; Gasparini, N.; Zhang, Z.; Liu, F.; Baran, D.; Tang, W. Nonfullerene Acceptor for Organic Solar Cells with Chlorination on Dithieno[3,2-b:2′,3′-d]pyrrol Fused-Ring. *ACS Energy Lett.* **2019**, *4*, 763−770.
(25) Kan, B.; Feng, H.; Yao, H.; Chang, M.; Wan, X.; Li, C.; Hou, J.; Chen, Y. A chlorinated low-bandgap small-molecule acceptor for organic solar cells with 14.1% efficiency and low energy loss. *Sci. China: Chem.* **2018**, *61*, 1307−1313.
(26) Li, S.; Ye, L.; Zhao, W.; Yan, H.; Yang, B.; Liu, D.; Li, W.; Ade, H.; Hou, J. A Wide Band Gap Polymer with a Deep Highest Occupied Molecular Orbital Level Enables 14.2% Efficiency in Polymer Solar Cells. *J. Am. Chem. Soc.* **2018**, *140*, 7159−7167.
(27) Yuan, J.; Zhang, Y.; Zhou, L.; Zhang, G.; Yip, H.-L.; Lau, T.-K.; Lu, X.; Zhu, C.; Peng, H.; Johnson, P. A.; Leclerc, M.; Cao, Y.; Ulanski, J.; Li, Y.; Zou, Y. Single-Junction Organic Solar Cell with over 15% Efficiency Using Fused-Ring Acceptor with Electron-Deficient Core. *Joule* **2019**, *3*, 1140−1151.
(28) Zhang, S.; Qin, Y.; Zhu, J.; Hou, J. Over 14% Efficiency in Polymer Solar Cells Enabled by a Chlorinated Polymer Donor. *Adv. Mater.* **2018**, *30*, 1800868.
(29) Li, X.; Pan, F.; Sun, C.; Zhang, M.; Wang, Z.; Du, J.; Wang, J.; Xiao, M.; Xue, L.; Zhang, Z. G.; Zhang, C.; Liu, F.; Li, Y. Simplified synthetic routes for low cost and high photovoltaic performance n-type organic semiconductor acceptors. *Nat. Commun.* **2019**, *10*, 519.
(30) Sun, C.; Pan, F.; Bin, H.; Zhang, J.; Xue, L.; Qiu, B.; Wei, Z.; Zhang, Z. G.; Li, Y. A low cost and high performance polymer donor material for polymer solar cells. *Nat. Commun.* **2018**, *9*, 743.
(31) Sirringhaus, H.; Brown, P. J.; Friend, R. H.; Nielsen, M. M.; Bechgaard, K.; Langeveld-Voss, B. M. W.; Spiering, A. J. H.; Janssen, R. A. J.; Meijer, E. W.; Herwig, P.; de Leeuw, D. M. Two-dimensional charge transport in self-organized, high-mobility conjugated polymers. *Science* **1998**, *280*, 1741−1744.
(32) Guo, X.; Cui, C.; Zhang, M.; Huo, L.; Huang, Y.; Hou, J.; Li, Y. High efficiency polymer solar cells based on poly(3-hexylthiophene)/indene-C70 bisadduct with solvent additive. *Energy Environ. Sci.* **2012**, *5*, 7943−7949.
(33) Holliday, S.; Ashraf, R. S.; Wadsworth, A.; Baran, D.; Yousaf, S. A.; Nielsen, C. B.; Tan, C. H.; Dimitrov, S. D.; Shang, Z.; Gasparini, N.; Alamoudi, M.; Laquai, F.; Brabec, C. J.; Salleo, A.; Durrant, J. R.; McCulloch, I. High-efficiency and air-stable P3HT-based polymer solar cells with a new non-fullerene acceptor. *Nat. Commun.* **2016**, *7*, 11585.
(34) Ma, W.; Yang, C.; Gong, X.; Lee, K.; Heeger, A. J. Thermally Stable, Efficient Polymer Solar Cells with Nanoscale Control of the Interpenetrating Network Morphology. *Adv. Funct. Mater.* **2005**, *15*, 1617−1622.
(35) Zhao, G.; He, Y.; Li, Y. 6.5% Efficiency of polymer solar cells based on poly(3-hexylthiophene) and indene-C(60) bisadduct by device optimization. *Adv. Mater.* **2010**, *22*, 4355−4358.
(36) Greve, D. R.; Apperloo, J. J.; Janssen, R. A. J. Synthesis and and Characterisation of Novel Regioregular Polythiophenes-Tuning the Redox Properties. *Eur. J. Org. Chem.* **2001**, *2001*, 3437−3443.
(37) Huo, L.; Chen, T. L.; Zhou, Y.; Hou, J.; Chen, H.-Y.; Yang, Y.; Li, Y. Improvement of Photoluminescent and Photovoltaic Properties of Poly(thienylene vinylene) by Carboxylate Substitution. *Macromolecules* **2009**, *42*, 4377−4380.
(38) Jo, J. W.; Jung, J. W.; Wang, H.-W.; Kim, P.; Russell, T. P.; Jo, W. H. Fluorination of Polythiophene Derivatives for High Performance Organic Photovoltaics. *Chem. Mater.* **2014**, *26*, 4214−4220.
(39) Zhang, M.; Guo, X.; Ma, W.; Ade, H.; Hou, J. A polythiophene derivative with superior properties for practical application in polymer solar cells. *Adv. Mater.* **2014**, *26*, 5880−5885.
(40) Zhang, M.; Guo, X.; Yang, Y.; Zhang, J.; Zhang, Z.-G.; Li, Y. Downwards tuning the HOMO level of polythiophene by carboxylate substitution for high open-circuit-voltage polymer solar cells. *Polym. Chem.* **2011**, *2*, 2900−2906.
(41) Blaskovits, J. T.; Bura, T.; Beaupré, S.; Lopez, S. A.; Roy, C.; de Goes Soares, J.; Oh, A.; Quinn, J.; Li, Y.; Aspuru-Guzik, A.; Leclerc,

DOI: 10.1021/acs.macromol.9b00793
Macromolecules 2019, 52, 4464−4474

M. A Study of the Degree of Fluorination in Regioregular Poly(3-hexylthiophene). *Macromolecules* **2017**, *50*, 162−174.
(42) Homyak, P. D.; Liu, Y.; Harris, J. D.; Liu, F.; Carter, K. R.; Russell, T. P.; Coughlin, E. B. Systematic Fluorination of P3HT: Synthesis of P(3HT-co-3H4FT)s by Direct Arylation Polymerization, Characterization, and Device Performance in OPVs. *Macromolecules* **2016**, *49*, 3028−3037.
(43) Qin, Y.; Uddin, M. A.; Chen, Y.; Jang, B.; Zhao, K.; Zheng, Z.; Yu, R.; Shin, T. J.; Woo, H. Y.; Hou, J. Highly Efficient Fullerene-Free Polymer Solar Cells Fabricated with Polythiophene Derivative. *Adv. Mater.* **2016**, *28*, 9416−9422.
(44) Zhang, H.; Li, S.; Xu, B.; Yao, H.; Yang, B.; Hou, J. Fullerene-free polymer solar cell based on a polythiophene derivative with an unprecedented energy loss of less than 0.5 eV. *J. Mater. Chem. A* **2016**, *4*, 18043−18049.
(45) Yao, H.; Qian, D.; Zhang, H.; Qin, Y.; Xu, B.; Cui, Y.; Yu, R.; Gao, F.; Hou, J. Critical Role of Molecular Electrostatic Potential on Charge Generation in Organic Solar Cells. *Chin. J. Chem.* **2018**, *36*, 491−494.
(46) Gao, Y.; Zhang, X.; Tian, H.; Zhang, J.; Yan, D.; Geng, Y.; Wang, F. High Mobility Ambipolar Diketopyrrolopyrrole-Based Conjugated Polymer Synthesized Via Direct Arylation Polycondensation. *Adv. Mater.* **2015**, *27*, 6753−6759.
(47) Kawashima, K.; Fukuhara, T.; Suda, Y.; Suzuki, Y.; Koganezawa, T.; Yoshida, H.; Ohkita, H.; Osaka, I.; Takimiya, K. Implication of Fluorine Atom on Electronic Properties, Ordering Structures, and Photovoltaic Performance in Naphthobisthiadiazole-Based Semiconducting Polymers. *J. Am. Chem. Soc.* **2016**, *138*, 10265−10275.
(48) Li, Z.; Jiang, K.; Yang, G.; Lai, J. Y.; Ma, T.; Zhao, J.; Ma, W.; Yan, H. Donor polymer design enables efficient non-fullerene organic solar cells. *Nat. Commun.* **2016**, *7*, 13094.
(49) Zhao, W.; Li, S.; Yao, H.; Zhang, S.; Zhang, Y.; Yang, B.; Hou, J. Molecular Optimization Enables over 13% Efficiency in Organic Solar Cells. *J. Am. Chem. Soc.* **2017**, *139*, 7148−7151.
(50) Uddin, M. A.; Kim, Y.; Younts, R.; Lee, W.; Gautam, B.; Choi, J.; Wang, C.; Gundogdu, K.; Kim, B. J.; Woo, H. Y. Controlling Energy Levels and Blend Morphology for All-Polymer Solar Cells via Fluorination of a Naphthalene Diimide-Based Copolymer Acceptor. *Macromolecules* **2016**, *49*, 6374−6383.
(51) Kranthiraja, K.; Long, D. X.; Sree, V. G.; Cho, W.; Cho, Y.-R.; Zaheer, A.; Lee, J.-C.; Noh, Y.-Y.; Jin, S.-H. Sequential Fluorination on Napthaleneamide-Based Conjugated Polymers and Their Impact on Charge Transport Properties. *Macromolecules* **2018**, *51*, 5530−5536.
(52) Tang, M. L.; Oh, J. H.; Reichardt, A. D.; Bao, Z. Chlorination: A General Route toward Electron Transport in Organic Semiconductors. *J. Am. Chem. Soc.* **2009**, *131*, 3733−3740.
(53) Hiszpanski, A. M.; Saathoff, J. D.; Shaw, L.; Wang, H.; Kraya, L.; Lüttich, F.; Brady, M. A.; Chabinyc, M. L.; Kahn, A.; Clancy, P.; Loo, Y.-L. Halogenation of a Nonplanar Molecular Semiconductor to Tune Energy Levels and Bandgaps for Electron Transport. *Chem. Mater.* **2015**, *27*, 1892−1900.
(54) Qu, S.; Wang, H.; Mo, D.; Chao, P.; Yang, Z.; Li, L.; Tian, L.; Chen, W.; He, F. Fine Tuning of Open-Circuit Voltage by Chlorination in Thieno[3,4-b]thiophene-Benzodithiophene Terpolymers toward Enhanced Solar Energy Conversion. *Macromolecules* **2017**, *50*, 4962−4971.
(55) Wang, H.; Chao, P.; Chen, H.; Mu, Z.; Chen, W.; He, F. Simultaneous Increase in Open-Circuit Voltage and Efficiency of Fullerene-Free Solar Cells through Chlorinated Thieno[3,4-b]-thiophene Polymer Donor. *ACS Energy Lett.* **2017**, *2*, 1971−1977.
(56) Zhang, Y.; Yao, H.; Zhang, S.; Qin, Y.; Zhang, J.; Yang, L.; Li, W.; Wei, Z.; Gao, F.; Hou, J. Fluorination vs.chlorination: a case study on high performance organic photovoltaic materials. *Sci. China: Chem.* **2018**, *61*, 1328−1337.
(57) Lee, W.-Y.; Oh, J. H.; Suraru, S.-L.; Chen, W.-C.; Würthner, F.; Bao, Z. High-Mobility Air-Stable Solution-Shear-Processed n-Channel Organic Transistors Based on Core-Chlorinated Naphthalene Diimides. *Adv. Funct. Mater.* **2011**, *21*, 4173−4181.
(58) Wu, Y.; An, C.; Shi, L.; Yang, L.; Qin, Y.; Liang, N.; He, C.; Wang, Z.; Hou, J. The Crucial Role of Chlorinated Thiophene Orientation in Conjugated Polymers for Photovoltaic Devices. *Angew. Chem., Int. Ed.* **2018**, *57*, 12911−12915.
(59) Tang, M. L.; Oh, J. H.; Reichardt, A. D.; Bao, Z. Chlorination: A General Route toward Electron Transport in Organic Semiconductors. *J. Am. Chem. Soc.* **2009**, *131*, 3733−3740.
(60) Chen, H.; Hu, Z.; Wang, H.; Liu, L.; Chao, P.; Qu, J.; Chen, W.; Liu, A.; He, F. A Chlorinated π-Conjugated Polymer Donor for Efficient Organic Solar Cells. *Joule* **2018**, *2*, 1623−1634.
(61) Lei, T.; Dou, J.-H.; Ma, Z.-J.; Liu, C.-J.; Wang, J.-Y.; Pei, J. Chlorination as a useful method to modulate conjugated polymers: balanced and ambient-stable ambipolar high-performance field-effect transistors and inverters based on chlorinated isoindigo polymers. *Chem. Sci.* **2013**, *4*, 2447−2452.
(62) Zhao, F.; Dai, S.; Wu, Y.; Zhang, Q.; Wang, J.; Jiang, L.; Ling, Q.; Wei, Z.; Ma, W.; You, W.; Wang, C.; Zhan, X. Single-Junction Binary-Blend Nonfullerene Polymer Solar Cells with 12.1% Efficiency. *Adv. Mater.* **2017**, *29*, 1700144.
(63) Heuvel, R.; Colberts, F. J. M.; Wienk, M. M.; Janssen, R. A. J. Thermal behaviour of dicarboxylic esterbithiophene polymers exhibiting a highopen-circuit voltage. *J. Mater. Chem. C* **2018**, *6*, 3731−3762.
(64) Zhang, Z.-G.; Qi, B.; Jin, Z.; Chi, D.; Qi, Z.; Li, Y.; Wang, J. Perylene diimides: a thickness-insensitive cathode interlayer for high performance polymer solar cells. *Energy Environ. Sci.* **2014**, *7*, 1966−1973.
(65) Carsten, B.; Szarko, J. M.; Son, H. J.; Wang, W.; Lu, L.; He, F.; Rolczynski, B. S.; Lou, S. J.; Chen, L. X.; Yu, L. Examining the effect of the dipole moment on charge separation in donor-acceptor polymers for organic photovoltaic applications. *J. Am. Chem. Soc.* **2011**, *133*, 20468−20475.
(66) Xu, X.; Li, Z.; Wang, J.; Lin, B.; Ma, W.; Xia, Y.; Andersson, M. R.; Janssen, R. A. J.; Wang, E. High-performance all-polymer solar cells based on fluorinated naphthalene diimide acceptor polymers with fine-tuned crystallinity and enhanced dielectric constants. *Nano Energy* **2018**, *45*, 368−379.
(67) Yang, P.; Yuan, M.; Zeigler, D. F.; Watkins, S. E.; Lee, J. A.; Luscombe, C. K. Influence of fluorine substituents on the film dielectric constant and open-circuit voltage in organic photovoltaics. *J. Mater. Chem. C* **2014**, *2*, 3278−3284.
(68) Clarke, T. M.; Durrant, J. R. Charge Photogeneration in Organic Solar Cells. *Chem. Rev.* **2010**, *110*, 6736−6767.
(69) Koster, L. J. A.; Shaheen, S. E.; Hummelen, J. C. Pathways to a New Efficiency Regime for Organic Solar Cells. *Adv. Energy Mater.* **2012**, *2*, 1246−1253.
(70) Liu, X.; Xie, B.; Duan, C.; Wang, Z.; Fan, B.; Zhang, K.; Lin, B.; Colberts, F. J. M.; Ma, W.; Janssen, R. A. J.; Huang, F.; Cao, Y. A high dielectric constant non-fullerene acceptor for efficient bulk-heterojunction organic solar cells. *J. Mater. Chem. A* **2018**, *6*, 395−403.
(71) Baumann, A.; Lorrmann, J.; Rauh, D.; Deibel, C.; Dyakonov, V. A new approach for probing the mobility and lifetime of photogenerated charge carriers in organic solar cells under real operating conditions. *Adv. Mater.* **2012**, *24*, 4381−4386.
(72) Nilsson, S.; Bernasik, A.; Budkowski, A.; Moons, E. Morphology and Phase Segregation of Spin-Casted Films of Polyfluorene/PCBM Blends. *Macromolecules* **2007**, *40*, 8291−8301.
(73) Feng, H.; Yi, Y. Q. Q.; Ke, X.; Yan, J.; Zhang, Y.; Wan, X.; Li, C.; Zheng, N.; Xie, Z.; Chen, Y. New Anthracene-Fused Nonfullerene Acceptors for High-Efficiency Organic Solar Cells: Energy Level Modulations Enabling Match of Donor and Acceptor. *Adv. Energy Mater.* **2019**, *9*, 1803541.
(74) Ye, L.; Hu, H.; Ghasemi, M.; Wang, T.; Collins, B. A.; Kim, J. H.; Jiang, K.; Carpenter, J. H.; Li, H.; Li, Z.; McAfee, T.; Zhao, J.; Chen, X.; Lai, J. L. Y.; Ma, T.; Bredas, J. L.; Yan, H.; Ade, H. Quantitative relations between interaction parameter, miscibility and function in organic solar cells. *Nat. Mater.* **2018**, *17*, 253−260.

DOI: 10.1021/acs.macromol.9b00793
Macromolecules 2019, 52, 4464−4474